

RESEARCH ARTICLE

Magnetometer Calibration and Missile Attitude Filtering Method Based on Energy Estimation

YAN XIAOLONG^{1,2}, BAI DUNZHUO³, ZHAO FUCHUN⁴, AND ZHANG WEI²¹College of Mechatronics Engineering, North University of China, Taiyuan 030051, China²Huaihai Industry Group Company Ltd., Changzhi 046000, China³Yuxi Industry Group Company Ltd., Nanyang 473000, China⁴Shandong Special Industry Group Company Ltd., Zibo 255000, China

Corresponding author: Yan Xiaolong (yanxl@nuc.edu.cn)

This work was supported in part by the China Postdoctoral Science Foundation under Project 2021M691987.

ABSTRACT Estimating the flying attitude of the missile body during flight is vitally important for the intelligent ammunition. The earlier and more accurate the posture information is obtained, the more conducive it is to the control process of the intelligent ammunition. The magnetometer is commonly used to measure the roll attitude of the missile. However, the cumbersome calibration steps and noise interference of the missile usually cause the delay in the attitude calculation and inaccurate measurement. To solve these issues, an adaptive reconfigurable unscented Kalman filter (ARUKF) method based on energy estimation is proposed. The magnetic field measured by the magnetometer is analyzed in real time based on the roll characteristic of the intelligent ammunition to achieve the initial calibration of the magnetometer parameters. With the obtained calibrated parameters, the filter state variables are estimated by establishing the residual estimation function in the UKF, which guides the reconstruction of the UKF to minimize the computational cost of the attitude estimation process. Simultaneously, the on-board computer system feeds back the action of the rudder system in real time to guide the configuration of the noise parameters in the UKF process, which can effectively reduce the interference of the magnetic field generated by the rudder system on the attitude estimation. The numerical simulation and experiments show that the proposed method performs better in terms of parameter convergence speed and estimation accuracy, compared with the traditional UKF method, which has great application prospect in the field of intelligent ammunition.


INDEX TERMS Energy estimation, unscented Kalman filter, state reconstruction, magnetic interference.

I. INTRODUCTION

With the development of the low-cost intelligent ammunition, rapid and low-cost measurement of the missile attitude has become one of the hotspots in the intelligent ammunition research. Apart from specific mission oriented discussions, the conducted researches for missile attitude measurement mainly focus on solving the following two problems: how to realize the high-precision attitude estimation under the premise of cost control, and how to reduce the amount of computation to complete real-time calculations on the low-cost processor [1], [2], [3]. Accordingly, a sound real-time algorithm becomes the key to the low-cost and accurate

attitude measurement scheme of the intelligent ammunition [4], [5].

Magnetometer is one of the low-cost attitude sensors that commonly used in intelligent munitions, since it has low power consumption, small size and strong anti-overload ability. However, the magnetometer has some inevitable errors in attitude estimation due to the manufacturing process and measurement principle of the magnetometer, resulting in inaccurate attitude information [6], [7], [8], [9], [10]. Therefore, it is necessary to calibrate the magnetometer properly before the attitude estimation [11], [12], [13]. On the other hand, the missile has a relatively complex electromagnetic environment. For example, the rudder system responsible for flight control can produce strong magnetic field noise signals during flight, which will cause the negative impact on the

The associate editor coordinating the review of this manuscript and approving it for publication was Mohammed Bait-Suwailam .

attitude estimation of the magnetometer, and should also be considered [14].

With the application of the magnetometers as the attitude sensors, many calibration and estimation algorithms have been proposed to improve the accuracy of the magnetometers [15], [16], [17]. However, in order to estimate the attitude of ammunition, the real-time capability of the calculation and the time variability of the error must be fully considered, and the calculation cost should be as low as possible.

Since the magnetic sensitive axis in the missile cross-section can obtain the sinusoidal variation of the geomagnetic component during the rapid roll of the missile, the “zero crossing method” of the magnetometer is initially proposed to measure the roll attitude of the missile [18], [19]. It has advantages of quick estimation of the roll attitude of the missile and simple calculation process. However, the solution accuracy of this method is not high enough to meet the requirements of the precious control of the ammunition. Some researchers have estimated the missile attitude through fitting the sinusoidal waveform obtained by the sensitive axis of the magnetometer to improve the solution accuracy [20], [21], [22]. However, the solving speed of the roll attitude is limited by the nonlinearity of the four-parameter fitting of the sinusoidal function [23]. Later, it is found that if the time information of the magnetometer measurement data is ignored, the data points of the ellipse can be obtained by the biaxial magnetometer on the rolling missile. According to the measurement principle of the magnetometer, the sensitivity error and nonorthogonal error of the magnetometer can be estimated by comparing the obtained ellipse data with the standard ellipse data. Thus, the relatively accurate measurement baseline of the magnetometer can be obtained to measure the flight attitude of the missile [24], [25], [26], [27]. Similarly, ignoring the time information, the data points of the ellipsoid can be obtained by the three-axis magnetometer, and the calibration parameters of the three-axis magnetometer can be calculated by using the ellipsoid fitting method. However, since the velocity direction of the missile rarely changes during flight, the output value of the sensitive axis of the magnetometer in the direction of the missile axis is almost constant in a short time, which is not conducive to ellipsoid fitting. Therefore, this kind of methods is more applicable to the aircrafts with large change ability in the velocity direction, such as unmanned aircraft [28], [29].

In order to further improve the accuracy of the magnetometer in estimating missile attitude, Soken et al. proposed the unscented Kalman filter (UKF) method to calculate the missile attitude [30], [31]. In this method, the TRIAD method combining multiple sensors was utilized to calibrate the sensors mainly based on the magnetometer. After obtaining the initial solution results, UKF was used to filter the measurement results online, which further improves the solution speed and accuracy. Yan et al. used ellipse fitting to preliminarily estimates the calibration parameters of the magnetometer, and set the results as the initial value of UKF for real-time estimation [32]. After the calibration parameters

of the magnetometer was converged steadily, UKF was simplified and reconfigured to quickly calculate the missile attitude. Thus, the solution speed was improved, while the solution accuracy of missile attitude at low CPU utilization was ensured.

The environment of the missile borne system is complex since the information measured by the magnetometer is not only the geomagnetic field generated by the earth, but also the electromagnetic field generated by other systems on the missile, which directly affects the measurement accuracy of the missile attitude [33], [34], [35], [36]. Some researchers used other types of sensors to relay measure the missile attitude once the magnetometer is disturbed [37], [35], [38]. Felipe et al. proposed a TRIAD-PBE attitude measurement scheme integrating the accelerometer and the magnetometer [39]. The reference information for calibrating the magnetometer was enriched with the information provided by the accelerometer information, which could partly reduce the influence of external interference on the attitude estimation. Yang et al. proposed the Adaptive Fading Square Root Unscented Kalman Filter algorithm by combining the three-axis accelerometer and the triaxial magnetometer, which could improve the self-adaptive ability after the noise was brought into the measurement process and reduce the computational complexity [40]. Feng combined the gyroscope and the magnetometer to extend the Kalman filter [41]. Accordingly, a disturbance index was proposed to characterize the magnitude of the external interference, and judge whether the gyroscope data was used to replace the magnetometer data to complete the attitude estimation.

Compared with the existing literature, a novel adaptive reconfigurable UKF (ARUKF) method is proposed to calibrate the magnetometer independently for accurately estimating the missile attitude in the strong interference environment. The main contributions of this article are as follows:

(1) A trigonometric function fitting method with four fast convergence parameters is proposed to fit the data obtained from the sensitive axis of the magnetometer in the cross-section of the missile body for estimating the missile attitude. In this step, the magnetic field vector measured by the magnetometer is approximately expressed as the energy under the accumulation of time. Thus, the initial calibration parameters of the magnetometer and missile attitude are obtained.

(2) The initial calibration parameters and attitude parameters are further filtered as the initial state variables of the UKF to construct a convergence evaluation function of all parameters. By estimating the time-varying characteristics of the initial calibration parameters and attitude parameters, the UKF algorithm is reconstructed after the convergence of partial parameters. Therefore, the calculation cost of the attitude estimation process can be reduced without reducing the measurement accuracy. When the calibration parameters change due to the external interference, the reconstructed function of the UKF can quickly judge and deal with the inaccurate calibration parameters.

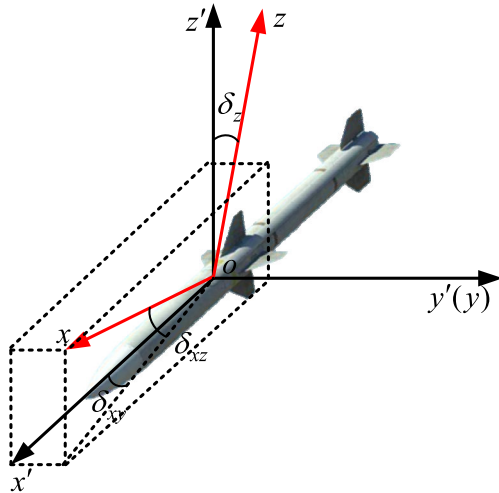


FIGURE 1. Model of the missile attitude measurement by the magnetometer.

(3) In order to solve the problem of external disturbance during the measurement of the magnetometer, the disturbing magnetic field caused by the alternating current generated by the rudder system in the missile is considered as the interference environment. The magnetometer components update the measurement noise parameters of the UKF in real time based on the control commands of the rudder system to match the current interference environment. Moreover, the reconstruction strategy of UKF is reactivated to reconfigure the measurement noise and the affected calibration parameters again to ensure the estimation accuracy of the missile attitude.

The rest of the paper is organized as follows. The mathematical model of the magnetometer is established in Section 2; the main steps of independent calibration and attitude measurement of the magnetometer are described in Section 3; the numerical simulation and experimental verification are demonstrated in Section 4; the conclusion is given in Section 5.

II. MATHEMATICAL MODEL OF MAGNETOMETER

The measurement model of a three-axis magnetometer can be described as:

$$H_m = (I_{3 \times 3} + D_s D_k D_n)^{-1} (L H_E + B_m) + w \quad (1)$$

where, $H_m = [H_{mx} \ H_{my} \ H_{mz}]^T$ is the measurement value of the magnetometer in the missile coordinate system, $H_E = [H_{Ex} \ H_{Ey} \ H_{Ez}]^T$ is the local magnetic vector calculated by IGRF 13th generation, $B_m = [B_{mx} \ B_{my} \ B_{mz}]^T$ is the measurement bias of the magnetometer, w is the measurement error of the magnetometer, D_s is the soft iron error of the missile platform, D_k is the scale factor of the sensitive axis of the magnetometer, and D_n is the non-orthogonal error angle of the sensitive axis of the magnetometer.

The model of the missile attitude measurement by the magnetometer is shown in Figure 1. In the diagram, Ox' , Oy' , Oz' axes respectively correspond to the x, y, z axes of the

missile body, where Ox' direction is the missile head direction. Ox, Oy, Oz axes are the x, y, z axes of the missile strap-down magnetometer, respectively. To reduce the calibration difficulty of the magnetometer within the feasible operation range, and the y of the missile body coincides with the y' of the magnetometer when the magnetometer is installed on the missile body. δ_{yz} is the error angle between the z of the magnetometer and the z' of the missile, and δ_{xz} is the error angle between the x of the magnetometer and the $x'y'$ plane of the missile. δ_{xy} is the error angle between the projection of the x axis of the magnetometer on the $x'y'$ plane and the x' axis of the missile.

w is the Gauss white noise with zero-mean, and described as follows:

$$E [w_i w_j^T] = I_{3 \times 3} w_m^2 \delta_{ij} \quad (2)$$

where, w_m is the standard deviation of the noise measured by the magnetometer, and δ_{ij} is the Kronecker symbol.

Ignoring the asymmetric soft iron error, D_s can be considered as a symmetric matrix with nine independent components. The calibration of the error is difficult to be completed online during the missile flight since it requires special maneuvering of the magnetometer in three axial directions. Generally, these nine parameters are obtained by placing the whole platform on the ground test bench, which can be described as:

$$D_s = \begin{bmatrix} D_{s11} & D_{s12} & D_{s13} \\ D_{s22} & D_{s21} & D_{s23} \\ D_{s31} & D_{s32} & D_{s33} \end{bmatrix} \quad (3)$$

The scale factor of the sensitive axis of the magnetometer D_k is the proportional error of the corresponding sensitive axis, which is an inherent characteristic error of the magnetometer and can be described as:

$$D_k = \begin{bmatrix} D_{kx} & 0 & 0 \\ 0 & D_{ky} & 0 \\ 0 & 0 & D_{kz} \end{bmatrix} \quad (4)$$

D_n as the non-orthogonal error of the sensitive axis of the magnetometer, is also an inherent characteristic error of the magnetometer and can be described as:

$$D_n = \begin{bmatrix} \cos(\delta_{xy}) \cos(\delta_{xz}) & \sin(\delta_{xy}) \cos(\delta_{xz}) & \sin(\delta_{xz}) \\ 0 & 1 & 0 \\ 0 & \sin(\delta_{yz}) & \cos(\delta_{yz}) \end{bmatrix} \quad (5)$$

III. RECONFIGURABLE UKF ALGORITHM BASED ON ENERGY ESTIMATION

A. INITIAL ESTIMATION OF THE CALIBRATION PARAMETERS OF THE MAGNETOMETER BASED ON ENERGY CAPTURE

The calibration algorithm of the magnetometer through the energy estimation based UKF is actually a method for calibrating the magnetometer and obtaining accurate attitude estimation. In the first phase, a trigonometric function fitting algorithm with low computation is used to quickly estimate

the error factors between the sensitive axes and the error factors of each sensitive axis of the magnetometer. It includes the initial estimation of all the error factors of the magnetometer and a preliminary calculation of the missile attitude, which are not accurate and need to be optimized.

Since the missile rotates continuously during flight, the output of the sensitive axis of the magnetometer on the cross-section of the missile can be further described as:

$$\begin{cases} H_{myi} = A_y \sin(2\pi \dot{\gamma} t_i + \zeta_y) + B_{my} \\ H_{mzi} = A_z \sin(2\pi \dot{\gamma} t_i + \frac{\pi}{2} + \zeta_y + \delta_{yz}) + B_{mz} \end{cases} \quad (6)$$

where, H_{myi} , H_{mzi} are the i^{th} magnetic sampling of the y-axis and z-axis of the magnetometer, t_i is the i^{th} sampling point, A_y , A_z are the peak value of the y-axis and z-axis of the magnetometer, and ζ_y is the initial phase of the y-axis of the magnetometer.

In the missile coordinate system, the changing of magnetic field can generate the electric field according to Maxwell's theory. Here, we consider that the changing magnetic field produces corresponding energy. The calibration parameters of the magnetometer and the initial missile attitude can be obtained by estimating the equation of energy. The sine fitting is utilized to complete the initial estimation of the equation (6). For the convenience of fitting, the energy equation is described as an improved form as shown in equation (7).

$$\begin{cases} H_{myi} = p_y \sin(2\pi \dot{\gamma} t_i) + q_y \cos(2\pi \dot{\gamma} t_i) + B_{my} \\ H_{mzi} = p_z \sin(2\pi \dot{\gamma} t_i) + q_z \cos(2\pi \dot{\gamma} t_i) + B_{mz} \end{cases} \quad (7)$$

During the missile flight, the magnetic components are mostly sampled with equal intervals by the missile-borne computer. Setting the average sampling rate to f_s , and the variable τ as:

$$\tau = 2\pi \left(\frac{\dot{\gamma}}{f_s} \right) \quad (8)$$

Based on the motion model of the missile and the mathematical model of the magnetometer, the output of two sensitive axes of the magnetometer in the missile cross-section can be described as follows:

$$\begin{cases} H_{myi} = p_y \sin(\tau i) + q_y \cos(\tau i) + B_{my} \\ H_{mzi} = p_z \sin(\tau i) + q_z \cos(\tau i) + B_{mz} \end{cases} \quad (9)$$

For the above equation, the optimal parameter $M_c = [p_y \ q_y \ B_{my} \ p_z \ q_z \ B_{mz} \ \tau]^T$ needs to be found to minimize the error between the value obtained by solving two sinusoidal equations and the output results of the corresponding sensitive axis of the magnetometer, which is generally estimated by the standard of square deviation. In general, the least square is used to fit unknown parameters in the study. Fitting of sinusoidal parameters is described in detail in IEEE Standard 1241-2010. Fitting of sinusoidal functions in the time domain can generally be divided into two situations: one is the three-parameter fitting of the sine functions with the prior information of frequency, and another is the four-parameter

fitting of the sine function without the priori information of frequency.

In this study, the frequency information corresponds to the roll velocity of the missile. For the multi-sensor integrated guidance ammunitions, the roll rate information of the missile can be provided by a gyroscope installed on the cross-section of the missile. So that the three-parameter fitting of the sine function can be further completed, and the calibration parameters of the magnetometer can be obtained accurately and quickly. However, for the low-cost intelligent ammunition with independent attitude measurement by the magnetometer, the magnetometer, as the only measurement component in the missile, cannot provide the roll velocity information of the missile without calibration. Therefore, the four-parameter fitting of the sine function is required.

During the fitting process, the parameters to be fitted continue to approach the true values. The system matrix is expanded by q derivation of τ from the fitted data:

$$D_i = \begin{bmatrix} \sin(\tau_{j-1}) & \cos(\tau_{j-1}) & 1 & D_{j,1} \\ \sin(2\tau_{j-1}) & \cos(2\tau_{j-1}) & 1 & D_{j,2} \\ \vdots & \vdots & \vdots & \vdots \\ \sin(N\tau_{j-1}) & \cos(N\tau_{j-1}) & 1 & D_{j,N} \end{bmatrix} \quad (10)$$

where, j is the number of the loop iteration, and $D_{j,i}$ can be described as

$$D_{j,1} = A_{j-1} i \cos(i\tau_{j-1}) - B_{j-1} i \cos(i\tau_{j-1}) \quad (11)$$

Especially, in the process of the least square fitting of parameters of the sine function, the fitting of amplitude A , offset B and initial phase angle C is linear, which means the accuracy of frequency determines the final fitting residual. However, when the frequency fitting needs to be considered at the same time, the fitting problem becomes a more complex non-linear problem, so the calculation cost and time cost will become the biggest obstacle to the solution accuracy.

To solve the problem, the frequency parameter of the sine function is firstly estimated. Fast Fourier Transform is generally used to estimate the frequency of the measured data. In this case, the maximum estimation error is $\Delta f = f_s/2N$. Although the rolling frequency of the missile can be obtained at a faster rate, this level of error will cause large errors in the other three parameters of the sine function, which can seriously affect the fast flying missiles. Therefore, more accurate parameters need to be provided in the initial estimation of the rolling frequency of the missile. Recent studies have demonstrated that interpolated fast Fourier transforms can perform more accurate frequency estimation of the discrete point data of the sine function. The rolling frequency of the missile in flight is a slowly changing parameter. In order to obtain frequency information under appropriate time and data volume conditions, Hanning window is selected as the fitting window function since it can provide a relatively accurate initial frequency estimation in a short period for data source of the sine function. The time domain range

can be described as:

$$w_i = 0.5 \left(1 - \cos \left(\frac{2\pi i}{N} \right) \right) \quad (12)$$

When the measurement data H_{mi} with required number are entered into the window function, the data frequency in the window function based on the interpolation points number n can be described as:

$$\mu = |FFT \{H_{mi} \cdot w_i, n\}| \quad (13)$$

After obtaining the initial rolling frequency value of the missile, further iteration of the frequency parameter is needed to obtain accurate roll angle parameters of the missile. However, the iteration process here can increase the calculation cost. In order to effectively predict the rolling frequency of the missile, the fitting result and the cost function σ of the measurement result are approximately considered as a quadratic function of the parameters to be fitted when approaching the optimal frequency parameter. In the four-parameter fitting of sine function, a 4-dimensional paraboloid is formed by p, q, τ, B_m and cost function σ when approaching the optimal parameters. If we only focus on the frequency parameter and the cross-section of 4-dimensional paraboloid, a parabola about the frequency parameter and cost function is obtained, in which the lowest point is the minimum value of cost function with respect to the frequency. The value of the abscissa corresponding to this point is the optimal value of the rolling frequency of the missile.

Parabolic fitting requires at least three coordinate points. For the magnetometer which is directly connected to a missile, the y-axis and z-axis are two sensitive axes that are theoretically orthogonal on the cross-section of the missile. Therefore, the rolling frequency information obtained in these two cycles are the same, and the frequency information obtained by FFT on the experimental data of the two sensitive axes are almost the same. In the parabolic fitting process, two points that are too close to each other on the curve have no positive effect on the fitting, so the average value of these two points is taken as a new data point $\bar{\tau}_{FFT}$ to be fitted. At the same time, $n-1$ points are generated near this point and marked as $\hat{\sigma}_k = a\tau_k^2 + b\tau_k + c$. The matrix equation is:

$$f_1(\tau_k) = S [a \ b \ c] \quad (14)$$

where, $f_1(\tau_k)$ is a vector of $n \times 1$, S is an $n \times 3$ -dimensional matrix, and M represents the number of samples.

The cost function is defined as

$$f_2(\tau_k) = \frac{1}{2} (S [a \ b \ c] - Y)^T (S [a \ b \ c] - Y) \quad (15)$$

where, Y is the output vector of the sample, so the quadratic relationship between the frequency and cost function can be described as:

$$[a \ b \ c]^T = (S^T S)^{-1} S^T Y \quad (16)$$

Based on the above description, the lowest point of the cost function represented by the parabola is the optimal selection

point for the rolling frequency of the missile.

$$\tau_{opt} = -\frac{b}{2a} \quad (17)$$

Here, the rolling angle frequency of the missile can be considered as an accurate parameter. According to the output signal of y and z axes of the magnetometer on the missile, the $X = [p_y \ q_y \ B_{my} \ p_z \ q_z \ B_{mz}]^T$ in the equation (9) can be solved according to the least square method:

$$D_{opt} = \begin{bmatrix} \sin(\tau_{opt}) & \cos(\tau_{opt}) & 1 \\ \sin(2\tau_{opt}) & \cos(2\tau_{opt}) & 1 \\ \vdots & \vdots & \vdots \\ \sin(N\tau_{opt}) & \cos(N\tau_{opt}) & 1 \\ & \cos(\tau_{opt}) & \sin(\tau_{opt}) & 1 \\ & \cos(2\tau_{opt}) & \sin(2\tau_{opt}) & 1 \\ & \vdots & \vdots & \vdots \\ & \cos(N\tau_{opt}) & \sin(N\tau_{opt}) & 1 \end{bmatrix} \quad (18)$$

B. CONFIGURATION OF UKF

At this point, the initial parameters of the sinusoidal transformed magnetic field are obtained based on the magnetometer on the rolling missile. In the second phase, UKF is used to process these inaccurate error information and attitude information to further obtain more accurate attitude estimation, and correct the calibration parameters of the magnetometer. UKF algorithm is selected here instead of other non-linear filter algorithms because there is still a large error after the first phase of preliminary estimation of the initial value, and UKF is undoubtedly the best choice when the parameters with large error is used as the initial value of the filter state.

The UKF process mainly consists of two phases, prediction phase and update phase. During the prediction phase, a set of sigma prediction points is generated.

The continuous nonlinear state equation of UKF can be described as:

$$X_k = f [X_{k-1}, u_{k-1}] + W_k \quad (19)$$

The measurement equation can be described as:

$$Y_k = h [X_k, k] + \Gamma V_k \quad (20)$$

The process noise W_k and observation noise V_k exist as linear additives in the system state equation and observation equation, and the variance matrix is Q_k and R_k respectively. Γ is the observation noise driving function. The working state of the magnetometer on the missile is complex and changeable, so the measurement error of the magnetometer can be influenced by the ambient temperature, vibration frequency and the state of the missile control mechanism. Therefore, the variance matrix R_k of the observation noise is constantly

changing during the working process of the magnetometer. To improve the filtering accuracy of UKF, the changing trend of the noise should be described. Since the pitch and yaw angles of the missile change slowly in most cases during flight, the theoretical value of the magnetometer sensitive axis (x-axis) in the direction of the missile axis can be considered a fixed value in a short time. This state is very stable relative to the rapid change of the measured value of the magnetometer sensitivity axis in the cross-section of the missile. Considering that the three axes of the magnetometer on the missile has the same hardware state and working environment, the observation noise of y-axis and z-axis can be estimated based on the real-time measurements of the x-axis. The drive matrix of the observation noise can be described as

$$\Gamma V_k = \begin{bmatrix} f_{yx}(P_k^x) \\ f_{zx}(P_k^x) \end{bmatrix} \quad (21)$$

In the above equation, f_{yx}, f_{zx} are the first-order function of the measurement noise of the y-sensitive axis and the z-sensitive axis of the magnetometer with respect to the x-sensitive axis. P_k^x is the variance matrix of the observation noise of the x-sensitive axis. In order to improve the accuracy and real-time of variance calculation, and ensure that the observation data of the x-sensitive axis of the magnetometer is almost invariant when solving the variance, a time window with a width of T_p is defined. P_k^x can be described as:

$$P_k^x = \sum_{i=0}^{T_p/f_s} \left(\left[H_{mx}^i - \hat{H}_{mx} \right] \left[H_{mx}^i - \hat{H}_{mx} \right]^T \right) \quad (22)$$

Step 1. Initialization

The calculation convergence process of UKF is sensitive to the initial value of the state variables. After the previous phases, the calibration parameters of the y, z sensitive axes of the magnetometer and the initial estimated parameters of the rolling movement of the missile are available. The initialized state vector can be described as:

$$\chi = [p_y \ q_y \ B_{my} \ p_z \ q_z \ B_{mz} \ \gamma_{Lr} \ \dot{\gamma}_{Lr} \ \ddot{\gamma}_{Lr}]^T \quad (23)$$

Step 2. Sigma Point Update

The $2n+1$ Sigma sample points are calculated at k-1 time as:

$$\begin{cases} \tilde{\chi}_{k-1}^{(0)} = \hat{\chi}_{k-1} \\ \tilde{\chi}_{k-1}^{(i)} = \hat{\chi}_{k-1} + \gamma (P_{k-1})_i \quad i = 1, 2, \dots, n \\ \tilde{\chi}_{k-1}^{(i)} = \hat{\chi}_{k-1} - \gamma (P_{k-1})_i \quad i = n+1, n+2, \dots, 2n \end{cases} \quad (24)$$

In the above equation, $\gamma = \sqrt{n+\lambda}$, $\lambda = \alpha^2(n+\kappa) - n$, where α is a very small value with a general range of $10^{-4} \leq \alpha \leq 1$, and $\kappa = 3 - n$. The β value is related to the distribution form of the state variables, and $\beta = 2$ for normal distribution.

Step3. Prediction Process

(1) Calculation of the one-step prediction model value at k-time as follows:

$$\begin{cases} \chi_{k/k-1}^{*(i)} = f \left[\tilde{\chi}_{k-1}^{(i)}, u_{k-1} \right] \quad i = 0, 1, 2, \dots, 2n \\ \hat{\chi}_{k/k-1} = \sum_{i=0}^{2n} W_i^{(m)} \tilde{\chi}_{k/k-1}^{*(i)} \\ P_{k/k-1} = \sum_{i=0}^{2n} W_i^{(c)} \left[\chi_{k/k-1}^{*(i)} - \hat{\chi}_{k/k-1} \right] \left[\chi_{k/k-1}^{*(i)} - \hat{\chi}_{k/k-1} \right]^T \\ \quad + Q_{k-1} \end{cases} \quad (25)$$

(2) Calculation of the one-step prediction augmented sample points at k-time as follows:

$$\begin{cases} \chi_{k/k-1}^{(i)} = \chi_{k/k-1}^{*(i)} \quad i = 0, 1, 2, \dots, 2n \\ P_{k/k-1} = \sum_{i=0}^{2n} W_i^{(c)} \left[\chi_{k/k-1}^{*(i)} - \hat{\chi}_{k/k-1} \right] \left[\chi_{k/k-1}^{*(i)} - \hat{\chi}_{k/k-1} \right]^T \\ \quad + Q_{k-1} \\ \chi_{k/k-1}^{(i)} = \chi_{k/k-1}^0 - \gamma \left(\sqrt{Q_{k-1}} \right)_{i-2n} \\ \quad i = 3n+1, 3n+2, \dots, 4n \\ Z_{k/k-1}^{(i)} = h \left[\chi_{k/k-1}^{(i)} \right] \quad i = 0, 1, 2, \dots, 4n \\ \hat{Z}_{k/k-1} = \sum_{i=0}^{4n} W_i^{(m)} Z_{k/k-1}^{(i)} \end{cases} \quad (26)$$

where, W is the weight of each sigma point.

$$\begin{aligned} W_0^{(m)} &= \frac{1}{2n+\lambda} \\ W_i^{(m)} &= \frac{1}{2(2n+\lambda)}, \quad i = 1, 2, 3, \dots, 4n \end{aligned} \quad (27)$$

Step4. Calculation of Gain Matrix as follows:

$$K_k = P_{(XZ)k/k-1} P_{(ZZ)k/k-1}^{-1} \quad (28)$$

where, $P_{(XZ)}$, $P_{(ZZ)}$ are the covariance matrices.

$$P_{(XZ)k/k-1} = \sum_{i=0}^{4n} W_i^{(c)} \left[\chi_{k/k-1}^{(i)} - \hat{\chi}_{k/k-1} \right] \left[Z_{k/k-1}^{(i)} - \hat{Z}_{k/k-1} \right]^T$$

$$P_{(ZZ)k/k-1} = \sum_{i=0}^{4n} W_i^{(c)} \left[Z_{k/k-1}^{(i)} - \hat{Z}_{k/k-1} \right] \times \left[Z_{k/k-1}^{(i)} - \hat{Z}_{k/k-1} \right]^T + R_k$$

$$\begin{aligned} W_i^{(c)} &= \frac{1}{2(2n+\lambda)} \quad i = 1, 2, 3, \dots, 4n \\ W_0^{(c)} &= \frac{\lambda}{2n+\lambda} + 1 - \alpha^2 + \beta \end{aligned} \quad (29)$$

Step5. Filter Value Update

$$\begin{aligned} \hat{\chi}_k &= \hat{\chi}_{k/k-1} + K_k \left[Z_k - Z_{k/k-1} \right] \\ P_k &= P_{k/k-1} - K_k P_{(zz)k/k-1} K_k^T \end{aligned} \quad (30)$$

By constructing the UKF, we can obtain more accurate state information.

C. FILTER RECONSTRUCTION

The calculation amount of UKF is proportional to the dimension of the estimated parameters. Reducing the calculation amount is one of the most effective means to promote the realization of engineering for on-board computers on missiles. Therefore, it is meaningful to effectively reduce the estimated state parameters at the appropriate time without losing the accuracy of the missile attitude solution.

In the above description, the state parameters include the intrinsic characteristic parameters of the magnetometer, the state characteristic parameters of the magnetometer, and the attitude parameters of the missile to be determined. Among them, the intrinsic characteristic calibration parameters p_y, q_y, p_z, q_z of the magnetometer are determined by the production and processing process of the magnetometer. These parameters are determined when the product is manufactured, and cannot be changed once it is primarily identified and calibrated. The state characteristic parameters B_{my}, B_{mz} of the magnetometer are determined by the magnetic field of its environment and the reset state of the device. When the interference magnetic field in the environment where the device is located is constant, these parameters will continue to be valid once the device is powered on and reset. However, when the external interference magnetic field changes due to some specific environment (here, it refers to the on-board rudder that is close to the magnetic intensity meter in the working state), these parameters will change considerably and must be recalibrated. The attitude information $\gamma_{Lr}, \dot{\gamma}_{Lr}, \ddot{\gamma}_{Lr}$ of the missile needs to be solved in real time during the control process, and the optimal freshness level must be guaranteed.

Accordingly, in the third phase, we divide the estimated state parameters into three levels. The first level is the movement attitude parameters of the missile, which can not be ignored and must be retained in the state vector in real time. The second level is the state characteristic parameters of the magnetometer. These two parameters need to be determined according to the flight conditions and the measurement accuracy of the magnetometer to determine whether they are necessary to exist in the estimated state vector. The third level is the intrinsic characteristic parameters of the magnetometer, which will completely exit the position of the estimated state vector once are accurately estimated.

The UKF scheme mentioned in the previous section is used to calibrate the measurement parameters of the state of the magnetometer 9 above, until the parameter converges to the optimal value under allowable conditions. The optimal parameter estimation state vector of each step in the first phase is defined as \hat{S}_{k+1} , and the measurement estimation equation can be obtained as:

$$\hat{S}_{k+1} = E^* \left[S_{k+1} / Z_0^{k+1} \right] \quad (31)$$

Since all parameter estimates use the same initial conditions and measurement data, the optimal estimation results for calibration parameters are relevant.

To facilitate the evaluation of the convergence of the estimates, the estimation residuals are defined as:

$$e_{k+1} = \hat{S}_{k+1} - S \quad (32)$$

where, S is the true value of the estimated quantity.

Define the covariance matrix of two adjacent estimation vectors \hat{S}_{k+1} and \hat{S}_k as P_{k+1}^s :

$$\begin{aligned} P_{k+1}^s &= E \left[(e_{k+1} - e_k) (e_{k+1} - e_k)^T \right] \\ &= E \left[e_{k+1} (e_{k+1})^T - e_{k+1} (e_k)^T - (e_{k+1})^T e_k + (e_k) (e_k)^T \right] \end{aligned} \quad (33)$$

In the above equation, $E [e_k (e_k)^T]$ and $E [e_{k+1} (e_{k+1})^T]$ are the optimal covariance matrices of the two consecutive optimal estimators \hat{S}_k and \hat{S}_{k+1} , respectively. In the filtering process of equation (23) to equation (30), the estimator \hat{S}_k of the filter parameters is based on the system state equation. Therefore, the covariance and cross-covariance of the initial errors can be considered equal:

$$E [e_{k+1} (e_k)^T] = E [e_{k+1} (e_{k+1})^T] \quad (34)$$

Equation (33) can be simplified as:

$$P_{k+1}^s = E [e_{k+1} (e_k)^T] - e_k (e_k)^T \quad (35)$$

According to the above discussion, the filter convergence rules can be set as:

$$R_{S,k+1}^2 = \left(\hat{S}_{k+1} - \hat{S}_k \right)^T \left(P_{k+1}^s \right)^{-1} \left(\hat{S}_{k+1} - \hat{S}_k \right) \leq \Delta_{\min} \quad (36)$$

where, Δ_{\min} is the pre-set minimum convergence value. At this point, it can be considered that the filter state has reached the convergence state. According to the UKF theory, \hat{S}_{k+1} conforms to the normal distribution, as well as $\hat{S}_{k+1} - \hat{S}_k$. So the statistic $R_{S,k+1}^2$ is a χ^2 distribution with r degrees of freedom (DOF) (r is the number of parameters of the filter state vector), and the threshold value of Δ_{\min} can be determined referring to the critical value table of χ^2 distribution. Therefore, the filter state variable (B_{my}, B_{mz}) of the second level and the filter state variable (p_y, q_y, p_z, q_z) of the third level can be considered as fixed values and no longer filtered, and only the parameters related to the roll attitude of the missile are remained in the filter state vector.

$$\chi = [\gamma_{Lr}, \dot{\gamma}_{Lr}, \ddot{\gamma}_{Lr}] \quad (37)$$

In this case, the filter state vector is reduced from 9-DOF to 3-DOF, which greatly reduces the computational cost of the on-board computer for the conventional UKF ($2n+1$ sigma points are calculated for each DOF). In this state, the state characteristic parameters B_{my}, B_{mz} of the magnetometer are considered as accurate values and are not estimated in real time. However, these two parameters are most likely to

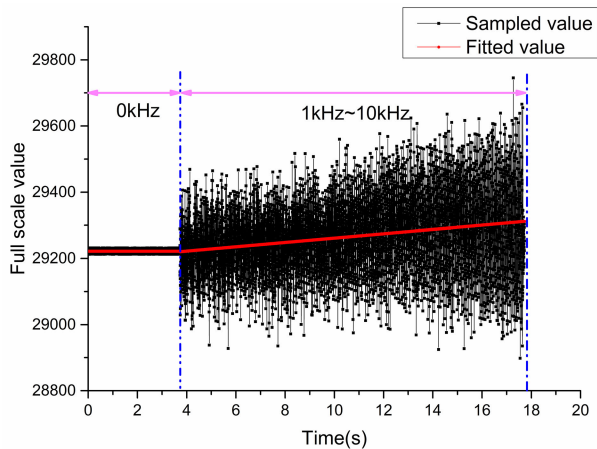


FIGURE 2. Interference of rudder system to static magnetic field measurement.

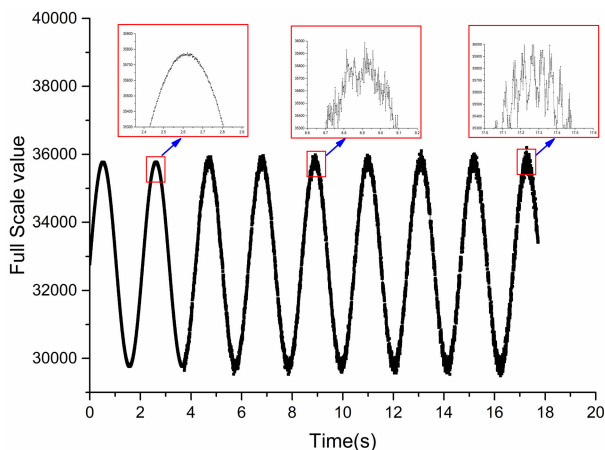


FIGURE 3. Disturbance of the rudder system to the measurement of the rotating magnetic field.

change with the state change of the missile. The rudder is one of the main factors that influences the magnetometer since the rudder is generally installed close to the magnetometer due to the size limitation of the missile. When the rudder is not working, the attitude measurement of the missile will not be affected because the magnetometer in this state has been calibrated in the previous calibration work. However, when the missile makes a maneuverable turn, the rudder will be energized according to the command requirements and the missile velocity. At this time, the changed electric field will generate a magnetic field, which will be added to the geomagnetic field vector to affect the original environmental magnetic field and cause the roll angle measurement error. At this point, the reconfigured algorithm should predict or sense this change and reconfigure back to the original magnetometer calibration filter scheme.

The impact of the on-board rudder system on the environmental magnetic field should be considered. When the conventional missile is launched against the ground target, the rudder system does not work through the full trajectory,

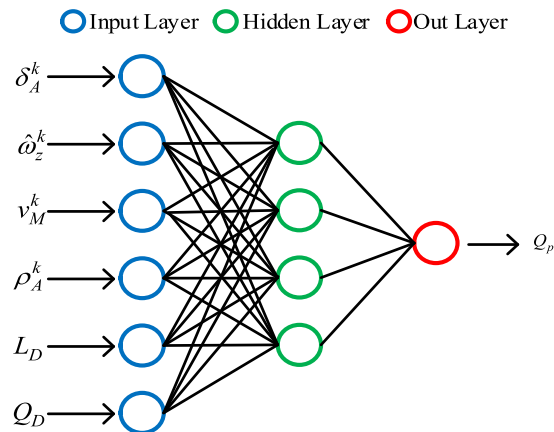


FIGURE 4. BP neural network estimation of interference magnetic field.

but depends on the requirements of the on-board computer of the missile. When the turning maneuver is required, the on-board computer will send out the corresponding rudder deflection instructions for each rudder. Combining with the roll attitude of the missile, the corresponding rudder deflection will produce a sinusoidal motion. The magnitude of the rudder deflection, the change frequency of the rudder system, and the air load determine the current in the rudder system, which reflects the magnitude of the generated interference magnetic field, as depicted in Fig. 2 and Fig. 3. The interference magnetic field can be described as:

$$\Delta B_{D-p} = f_{BL}(\delta_A, \omega_z, v_M, \rho_A, L_D, Q_D) \quad (38)$$

where δ_A is the rudder deflection value, ω_z is the angular velocity of the missile around the x-axis, v_M is the missile flight speed, ρ_A is the air density in the missile flight space, L_D is the distance from the missile axis where the rudder is installed to the magnetometer, and Q_D is the control noise of the rudder. The above six input factors all influence the magnetometer measurement. Therefore, the intensity of the interference magnetic field must be determined to reconstruct the measurement noise of the filter process to ensure the accuracy and smoothness of the filtering results. For the same type of missile, the missile body material, the motor model and the magnetometer model used are the same. Based on this characteristic, Back Propagation (BP) neural network algorithm is proposed to estimate the interference magnetic field in real time.

As shown in Fig. 4, the input layer nodes contain six factors mentioned above, among which accurate measurement values of ω_z cannot be provided. Here, the γ_{Lr} , $\dot{\gamma}_{Lr}$, $\ddot{\gamma}_{Lr}$ information from the previous phase is used for quadratic function fitting:

$$\hat{\omega}_z^k = \gamma_{Lr}^L + \dot{\gamma}_{Lr}^L * \Delta t + \ddot{\gamma}_{Lr}^L \Delta t^2 / 2 \quad (39)$$

The output layer node is the interference magnetic field generated by the rudder system, and the hidden layer has four nodes. The Logsig type in the Sigmoid function is selected as the driving function for the hidden layer, which is described

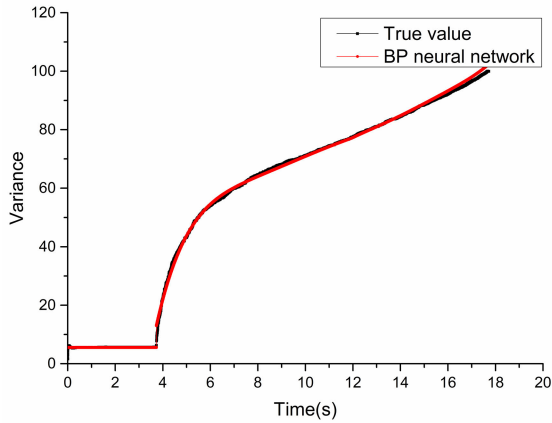


FIGURE 5. Estimation results of magnetic field noise by bp neural network.

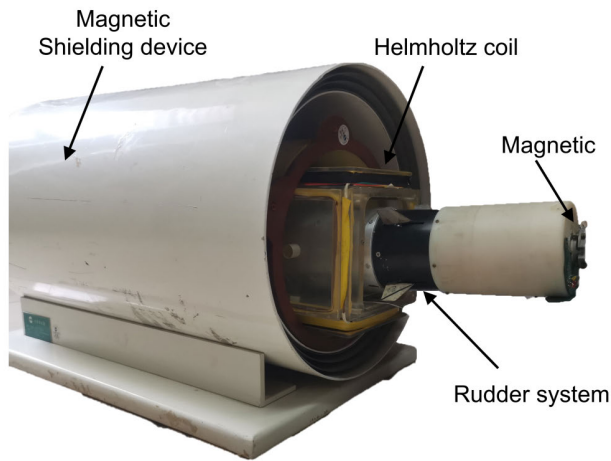


FIGURE 6. Hardware-in-loop simulation platform part a.

as:

$$\text{Logsig}(x) = 1/(1 + e^{-x}) \quad (40)$$

The linear Purelin function is selected for the output layer, which is described as:

$$\text{purelin}(x) = x \quad (41)$$

The input data X_{input} and output data Q_{output} from the semi-physical simulation model is selected as training data to build the evaluation function:

$$\epsilon_k = \sum (\hat{Q}_{output}^k - Q_{output}^k)^2 \quad (42)$$

After obtaining the measured noise value of the reconstructed filter, As shown in Fig. 5, the state vector of UKF is configured as:

$$\chi = [B_{my} \ B_{mz} \ \gamma_{Lr} \ \dot{\gamma}_{Lr} \ \ddot{\gamma}_{Lr}] \quad (43)$$

It is possible to switch back to the attitude filter after the filter converges to the new value of the calibration parameter.

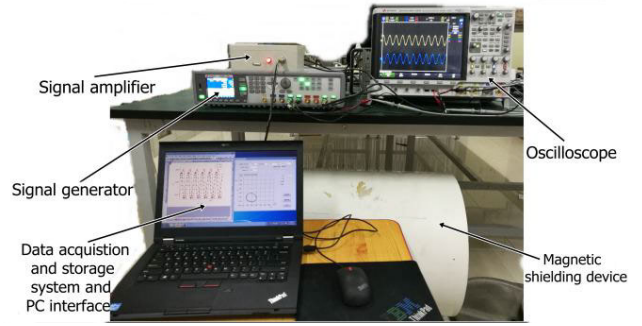


FIGURE 7. Hardware-in-loop simulation platform part b.

IV. SIMULATION EXPERIMENT

A. HARDWARE-IN-LOOP SIMULATION

The Hardware-in-loop simulation platform for the magnetometer attitude measurement is established based on the proposed ARUKF scheme. The attitude measurement compartment with magnetometer, rudder system compartment and on-board computer compartment are integrated to form the test body of the Hardware-in-loop simulation, as shown in Fig. 6 and Fig. 7. The compartments of the test body contain no ferromagnetic materials except the motor in the rudder to ensure the authenticity of the experiment. The distance between the magnetometer and the rudder compartment is $L_D = 110mm$. The attitude measurement section is all placed in the Helmholtz coil, which is used to generate known measured data. All the test subjects and the Helmholtz coil are placed in the magnetic shield barrel to isolate the external geomagnetic field and the possible interference magnetic fields.

The Helmholtz coil is used to generate a magnetic field with strength of $|H_E| = 0.5Gs$ and rotating along the axis of the projectile in the magnetic shielding barrel to simulate the rolling movement of the missile during flight. During the working process of the simulation system, the magnetic field is kept in the rotating state for 1~50s, and the rudder system is kept in the non-working state. The on-board computer controls the rudder system to generate control force in a constant direction in the period of 50s~80s, and then the missile returns to the uncontrolled state in 80~120s, as shown in Fig. 8.

Fig. 9 to Fig. 11 show that during the working process of the attitude measurement system, in the initial convergence phase, the trigonometric function fitting on the y-axis and the z-axis measurement data are respectively performed by the proposed algorithm scheme. So that the calibration parameters of the magnetometer can converge to a certain accuracy range at a faster speed compare to the traditional UKF algorithm which directly takes the nominal value of the calibration parameters as the initial filter value. In the continuous filtering phase, the trigonometric function fitting is utilized in the proposed scheme to obtain the calibration parameter results as the initial filtering value and ensure stable work of the filtering system, which has the similar working efficiency

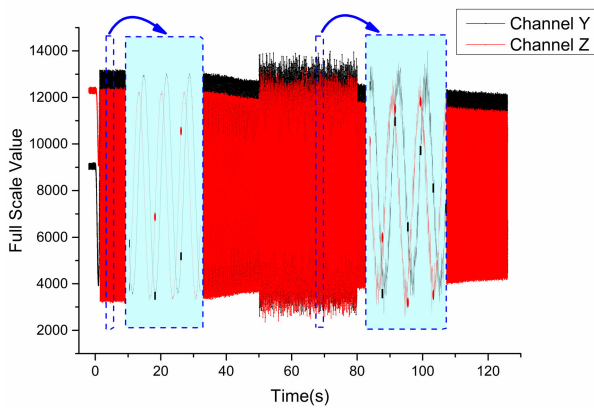


FIGURE 8. Magnetic field simulation data.

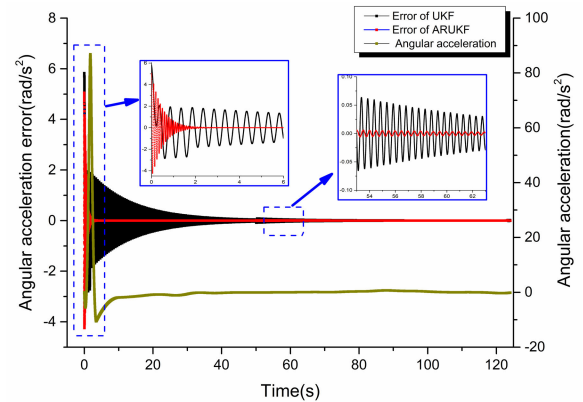


FIGURE 11. Estimation error of roll angle acceleration of missile body.

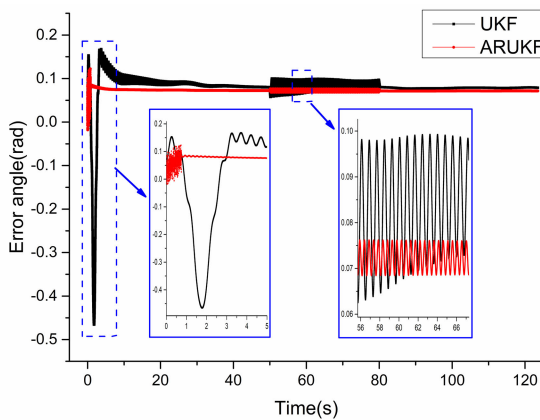


FIGURE 9. Estimation error of rolling angle of missile body.

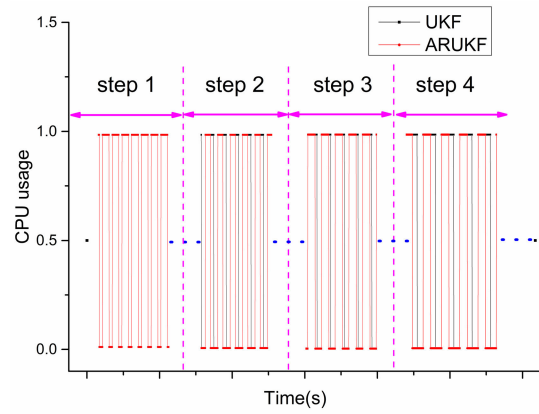


FIGURE 12. CPU utilization of onboard computer in different phases.

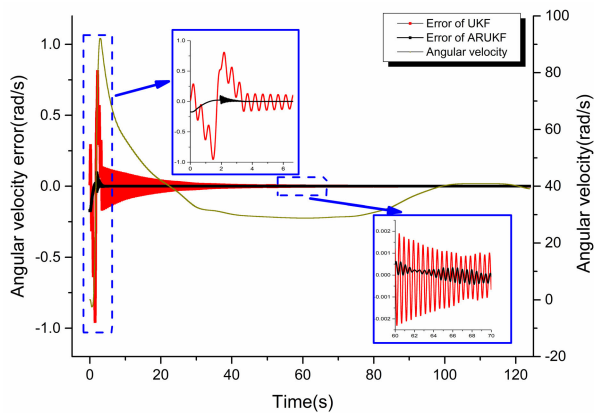


FIGURE 10. Estimation error of rolling angle velocity of missile body.

as the conventional UKF. After the rudder system on the missile starts to work, the proposed scheme reconstructs the UKF state vector and the measurement noise parameters in time according to the control instructions sent by the on-board computer to the rudder system. In this process, the roll attitude measurements of the missile are almost unaffected. Although the traditional UKF scheme has been filtering and estimating the calibration parameters of the magnetometer in full state, the measurement noise parameters have not been reconstructed and compensated in time in the process, which makes the large noise interference in the measurements of the

missile roll attitude. When the rudder system on the missile stops working, the proposed scheme reconstructs the state vector and measurement noise parameters according to the control instructions of the rudder output by the on-board computer. After the calibration parameters are stable, it can return to the UKF filtering scheme with low computation. However, the traditional UKF scheme is still in the full state filtering process at this time, and the roll attitude estimation of the missile returns to the original accuracy when there is no noise generated by the actuator system.

The calculation cost of the proposed scheme is the main basis for whether it can realize engineering implementation. To estimate the calculation amount of the two different algorithms, two attitude measurement scheme programs are executed respectively in the same hardware system, and the operation time of the functions in the scheme are monitored. So that the operation costs of the two schemes under the same state conditions can be obtained. It can be seen from Fig. 12 that the proposed scheme in the initial convergence phase (the first phase) has approximately the same computational complexity as the traditional UKF algorithm. When the magnetometer calibration parameter data is judged to be converged (the second phase), the calculation cost of the proposed scheme is significantly reduced due to the reconstruction of the state quantities. When the rudder system starts

TABLE 1. Magnetic field simulation data parameters.

Calibration parameters	Baseline of Y-axis	Baseline of Z-axis	Scale factor of peak value	Non-orthogonal error angle	Measurement noise (excluding rudder)	Measurement noise (including rudder)	sampling frequency
unit	FS	FS	1	deg	FS	FS	Hz
Nominal value	8192	8192	1	0	0	0	500
True value	8300	7800	1.0641	9.0	100	700	500

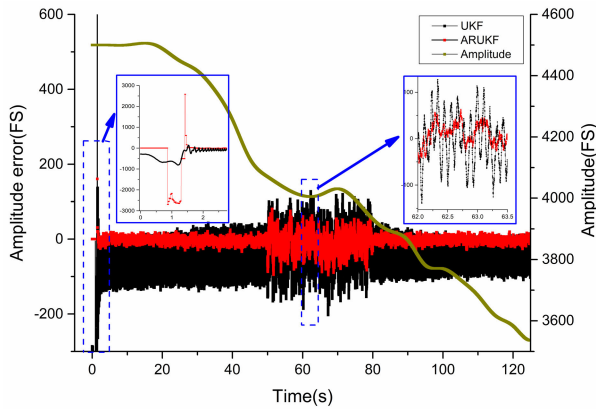


FIGURE 13. Amplitude estimation error.

to work, the state vector of the proposed scheme is further reconstructed (the third phase), but the inherent characteristic parameters of the magnetometer are still not included, and the calculation cost is still lower than that of the traditional UKF. When the rudder system stops working, the UKF of the proposed scheme further reduces the calculation cost and only the roll attitude of the missile is estimated (the fourth phase). In contrast, the traditional UKF has maintained a consistent high calculation cost in the whole process.

B. NUMERICAL SIMULATION

In the established semi-physical simulation system, the attitude measurement compartment, the rudder system compartment, the on-board computer compartment and the generated rotating magnetic field have all relatively restored the process of measuring the roll attitude of the missile through the magnetometer during flight. The measured roll angle displacement, angular velocity and angular acceleration are compared with the data of the generated rotating magnetic field to verify the correctness of the proposed algorithm. However, the accurate values of the calibration parameters of the magnetometer can not be obtained due to the small errors generated during the process of processing and packaging. To solve the problem, the complete numerical simulation model for measuring attitude of the magnetometer is established, and the error parameters of the magnetometer are pre-designed into the simulation model. By this way, the calibration parameters of the magnetometer obtained by the proposed algorithm can be compared and analyzed based on the true values.

Here the true values of simulation parameters are set as: Y-axis peak value to 8000 (full scale value), z-axis peak

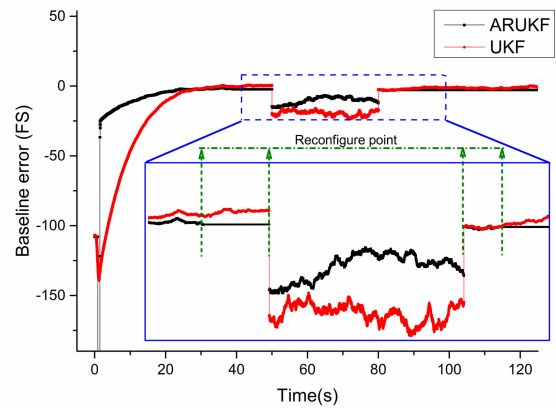


FIGURE 14. Baseline estimation error.

value to 7800 (full scale value), baseline of Y-axis to 32768, baseline of z-axis to 33520, non-orthogonal error angle to 8.6 deg.

In the above numerical simulation experiments, as the pitch angle and the yaw angle of the missile are constantly changing, the measured amplitude of the magnetometer is concomitantly changing while other parameters of the magnetometer (baseline, scale factor, non-orthogonal error angle) are constant. Accordingly, only the curve of amplitude changing with time is shown in Fig. 13, while other parameter estimation results are demonstrated as error values. As shown in figure a, after the missile is launched, the proposed ARUKF scheme completes the initial fitting of the amplitude parameters in a relatively short time, and then quickly turns to the real-time filtering phase. With the continuous change of the measured amplitude, the proposed ARUKF can still maintain the convergence state of the estimated value. After the rudder system starts to work, due to the increase of measurement noise, both of the traditional UKF and the proposed ARUKF scheme have a considerable impact on the estimated value of amplitude. However, the filtering effect of ARUKF is obviously better than that of the traditional UKF. Since the estimation process of the baseline of y-axis and z-axis are similar, as an example, the estimation result of y-axis baseline is shown in Fig. 14. In the initial phase, the calibration parameters are converged quickly by the fast fitting method based on energy estimation. When it converges to a certain accuracy, the UKF reconstruction condition is activated by the evaluation function. At this time, the proposed ARUKF scheme considers that the baseline parameters are temporarily constant and will not be estimated in a short time. After the rudder system starts to work, the magnetometer is disturbed by noise, and the baseline parameters are changed

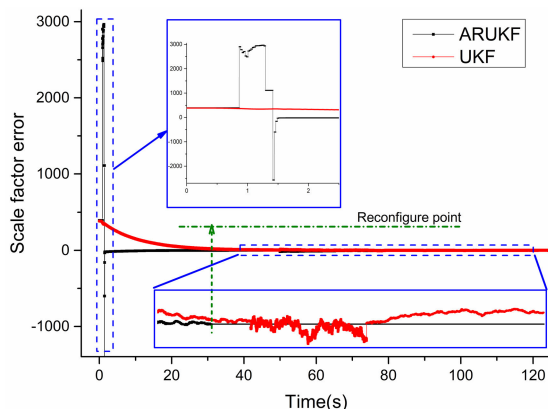


FIGURE 15. Scale factor estimation error.

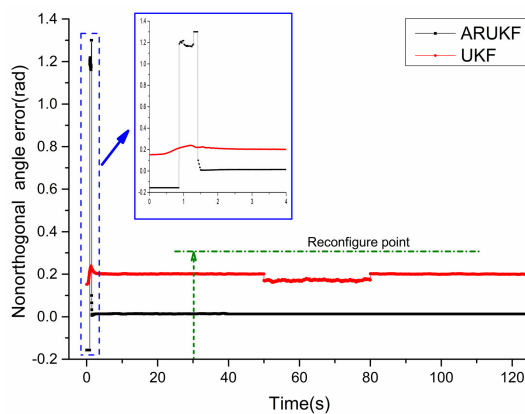


FIGURE 16. Nonorthogonal angle estimation error.

and re-incorporated into the UKF. Until the rudder system stops working, the baseline parameters are re-estimated to a constant value and then exit the UKF. During the whole process of baseline estimation, the proposed ARUKF scheme is obviously superior to the traditional UKF. Fig. 15 and Fig. 16 describe the estimation process of the scale factor errors and non-orthogonal angle errors of the magnetometer, respectively. Both of these two calibration parameters are inherent properties of the magnetometer and will not be changed with the change of the external environment once determined. Therefore, in the first phase, relatively accurate parameter estimates can be obtained quickly depending on the fast convergence characteristics of the proposed scheme. With the UKF reconstruction activated by evaluation function, the scale factor and non-orthogonal error angles are removed from the UKF. In contrast, the traditional UKF performs the filtering of the two parameters throughout the process, which may introduce unnecessary estimation errors when the rudder system works.

V. CONCLUSION

This paper presents a real-time filtering scheme for the independent calibration of magnetometers and the accurate measurement of missile roll attitude. The accurate roll attitude information can be obtained and provided to the missile even in the case of external interference, thus has strong robustness

to the uncertainty and measurement noise caused during the whole measurement process. In the proposed ARUKF scheme based on energy estimation, the potential energy of the magnetic field captured by cutting the geomagnetic field through missile rolling is used to quickly calibrate and measure the attitude measurement component of the magnetometer. Then, according to the time-varying characteristics of the parameters to be calibrated of the magnetometer, the adaptive strategy is used to calibrate the parameters by integrated filter under multiple states, which further reduces the calculation cost of the on-board computer. In addition, to overcome the interference of the rudder system to the attitude measurement components, a prediction scheme of the magnetometer measurement noise based on BP neural network is proposed, which provides reconstruction criteria for adaptive reconfigurable UKF and further improves the filtering performance under the uncertain conditions during the missile flight process. Numerical simulation experiments and Hardware-in-the-loop simulation experiments show that the proposed ARUKF scheme based on energy estimation can achieve higher calibration accuracy of the magnetometer and measurement accuracy of the roll attitude than the existing conventional filtering schemes, and has higher robustness to deal with the uncertainties and non-Gaussian measurement noise during flight process.

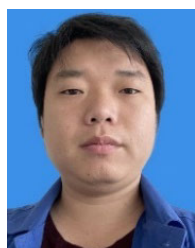
REFERENCES

- [1] G. Huang, B. K. Taylor, and D. Akopian, "A low-cost approach of magnetic field-based location validation for global navigation satellite systems," *IEEE Trans. Instrum. Meas.*, vol. 68, no. 12, pp. 4937–4944, Dec. 2019.
- [2] L. An, L. Wang, N. Liu, J. Fu, and Y. Zhong, "A novel method for estimating pitch and yaw of rotating projectiles based on dynamic constraints," *IEEE Sensors*, vol. 19, no. 23, pp. 1–21, Nov. 2019.
- [3] D. Long, X. Zhang, X. Wei, Z. Luo, and J. Cao, "A fast calibration and compensation method for magnetometers in strap-down spinning projectiles," *Sensors*, vol. 18, no. 12, p. 4157, Nov. 2018.
- [4] R. Alimi, E. Fisher, A. Ivry, A. Shavit, and E. Weiss, "Low power in situ AI calibration of a three-axial magnetic sensor," *IEEE Trans. Magn.*, vol. 55, no. 7, pp. 1–7, Jul. 2019.
- [5] P. Alken, N. Olsen, and C. C. Finlay, "Co-estimation of geomagnetic field and in-orbit fluxgate magnetometer calibration parameters," *Earth, Planets Space*, vol. 72, no. 1, pp. 1–32, Apr. 2020.
- [6] Y. Adachi, M. Higuchi, D. Oyama, Y. Haruta, S. Kawabata, and G. Uehara, "Calibration for a multichannel magnetic sensor array of a magnetospinography system," *IEEE Trans. Magn.*, vol. 50, no. 11, pp. 1–4, Nov. 2014.
- [7] P. Beran, M. Klohn, and H.-P. Hohe, "Measurement characteristics of different integrated three-dimensional magnetic field sensors," *IEEE Magn. Lett.*, vol. 10, pp. 1–5, 2019.
- [8] S. Angelopoulos, P. Vourna, A. Ktena, P. Tsarabaris, and E. Hristoforou, "Design and development of a new magnetometer calibration device," *IEEE Trans. Magn.*, vol. 55, no. 1, pp. 1–4, Jan. 2019.
- [9] J. J. Beato-López, I. Royo-Silvestre, and C. Gómez-Polo, "Micrometric non-contact position magnetoimpedance sensor," *J. Magn. Magn. Mater.*, vol. 465, pp. 489–494, Nov. 2018.
- [10] T. Beravs, S. Begus, J. Podobnik, and M. Munič, "Magnetometer calibration using Kalman filter covariance matrix for online estimation of magnetic field orientation," *IEEE Trans. Instrum. Meas.*, vol. 63, no. 8, pp. 2013–2020, Aug. 2014.
- [11] F. Cui, D. Gao, and J. Zheng, "Magnetometer-based orbit determination via fast reconstruction of three-dimensional decoupled geomagnetic field model," *J. Spacecraft Rockets*, vol. 58, no. 5, pp. 1374–1386, Sep. 2021.
- [12] V. V. Davydov, V. I. Dudkin, and A. Y. Karseev, "A two-channel navigation nuclear-magnetic magnetometer for remote control of the magnetic-field induction," *Instrum. Experim. Techn.*, vol. 58, no. 6, pp. 787–793, Nov. 2015.

- [13] H. Dai, C. Hu, S. Su, M. Lin, and S. Song, "Geomagnetic compensation for the rotating of magnetometer array during magnetic tracking," *IEEE Trans. Instrum. Meas.*, vol. 68, no. 9, pp. 3379–3386, 2019.
- [14] X. Dong, G. Chen, X. Tian, and X. Yan, "Real-time estimation of roll angles by magnetometer based on two-step adaptive Kalman filter," *Measurement*, vol. 198, Jul. 2022, Art. no. 111349.
- [15] Y. Huang and L. H. Wu, "Two-step complete calibration of magnetic vector gradiometer based on functional link artificial neural network and least squares," *IEEE Sensors J.*, vol. 16, no. 11, pp. 4230–4237, Jun. 2016.
- [16] T. Inamori, R. Hamaguchi, K. Ozawa, P. Saisutjarit, N. Sako, and S. Nakasuka, "Online magnetometer calibration in consideration of geomagnetic anomalies using Kalman filters in nanosatellites and microsatellites," *J. Aerosp. Eng.*, vol. 29, no. 6, Nov. 2016, Art. no. 04016046.
- [17] M. Janosek, M. Dressler, V. Petrucha, and A. Chirtsov, "Magnetic calibration system with interference compensation," *IEEE Trans. Magn.*, vol. 55, no. 1, pp. 1–4, Jan. 2019.
- [18] F. Plaschke, H.-U. Auster, D. Fischer, K.-H. Fornaçon, W. Magnes, I. Richter, D. Constantinescu, and Y. Narita, "Advanced calibration of magnetometers on spin-stabilized spacecraft based on parameter decoupling," *Geoscientific Instrum., Methods Data Syst.*, vol. 8, no. 1, pp. 63–76, Feb. 2019.
- [19] T. M. Roberts, K. A. Lynch, R. E. Clayton, M. E. Disbrow, and C. J. Hansen, "Magnetometer-based attitude determination for deployed spin-stabilized spacecraft," *J. Guid., Control, Dyn.*, vol. 40, no. 11, pp. 2941–2947, Nov. 2017.
- [20] P. Mahavarkar, J. John, V. Dhapre, V. Dongre, and S. Labde, "Tri-axial square Helmholtz coil system at the alibag magnetic observatory: Upgraded to a magnetic sensor calibration facility," *Geoscientific Instrum., Methods Data Syst.*, vol. 7, no. 2, pp. 143–149, Apr. 2018.
- [21] Z. Jiang, D. Zhang, and G. Lu, "Radial artery pulse waveform analysis based on curve fitting using discrete Fourier series," *Comput. Methods Programs Biomed.*, vol. 174, pp. 25–31, Jun. 2019.
- [22] P. Händel, "Amplitude estimation using IEEE-STD-1057 three-parameter sine wave fit: Statistical distribution, bias and variance," *Measurement*, vol. 43, no. 6, pp. 766–770, 2010.
- [23] T. Funck and T. Spiegel, "Verification of low frequency AC–DC transfer differences of thermal converters using sampling with sine-wave fit," *Meas. Sci. Technol.*, vol. 26, no. 9, Jul. 2015, Art. no. 095901.
- [24] G. Fedele, L. D'Alfonso, and G. D'Aquila, "Magnetometer bias finite-time estimation using gyroscope data," *IEEE Trans. Aerosp. Electron. Syst.*, vol. 54, no. 6, pp. 2926–2936, Dec. 2018.
- [25] J. Jung, J. Park, J. Choi, and H.-T. Choi, "Autonomous mapping of underwater magnetic fields using a surface vehicle," *IEEE Access*, vol. 6, pp. 62552–62563, 2018.
- [26] W.-W. Kao and C.-L. Tsai, "Adaptive and learning calibration of magnetic compass," *Meas. Sci. Technol.*, vol. 17, no. 11, pp. 3073–3082, Nov. 2006.
- [27] W. Lv, Y. Kang, and J. Qin, "Indoor localization for skid-steering mobile robot by fusing encoder, gyroscope, and magnetometer," *IEEE Trans. Syst., Man, Cybern. Syst.*, vol. 49, no. 6, pp. 1241–1253, Jun. 2019.
- [28] M. O. Archer, T. S. Horbury, P. Brown, J. P. Eastwood, T. M. Oddy, B. J. Whiteside, and J. G. Sample, "The MAGIC of CINEMA: First in-flight science results from a miniaturised anisotropic magnetoresistive magnetometer," *Annales Geophysicae*, vol. 33, no. 6, pp. 725–735, Jun. 2015.
- [29] C. Chesneau, R. Robin, H. Meier, M. Hillion, and C. Prieur, "Calibration of a magnetometer array using motion capture equipment," *Asian J. Control*, vol. 21, no. 4, pp. 1459–1469, Jul. 2019.
- [30] H. E. Söken and S. Sakai, "Attitude estimation and magnetometer calibration using reconfigurable TRIAD plus filtering approach," *Aerosp. Sci. Technol.*, vol. 99, pp. 1–10, Apr. 2020.
- [31] H. E. Söken and S.-I. Sakai, "Real-time attitude-independent magnetometer bias estimation for spinning spacecraft," *J. Guid., Control, Dyn.*, vol. 41, no. 1, pp. 276–279, Jan. 2018.
- [32] X. Yan, G. Chen, and X. Tian, "Two-step adaptive augmented unscented Kalman filter for roll angles of spinning missiles based on magnetometer measurements," *Meas. Control*, vol. 51, nos. 3–4, pp. 73–82, Apr. 2018.
- [33] J. L. Crassidis and Y. Cheng, "Three-axis magnetometer calibration using total least squares," *J. Guid., Control, Dyn.*, vol. 44, no. 8, pp. 1410–1424, Aug. 2021.
- [34] D. Cilden-Guler and C. Hajiyev, "SVD-aided EKF attitude estimation with UD factorized measurement noise covariance," *Asian J. Control*, vol. 21, no. 4, pp. 1423–1432, Jul. 2018.
- [35] J. K. Lee and T. H. Jeon, "Magnetic condition-independent 3D joint angle estimation using inertial sensors and kinematic constraints," *Sensors*, vol. 19, no. 24, p. 5522, Dec. 2019.
- [36] F. J. Nieves, A. Bayón, and F. Gascón, "Optimization of the magnetic field homogeneity of circular and conical coil pairs," *Rev. Sci. Instrum.*, vol. 90, no. 4, Apr. 2019, Art. no. 045120.
- [37] M. Muraccini, A. Mangia, M. Lannocca, and A. Cappello, "Magnetometer calibration and field mapping through thin plate splines," *Sensors*, vol. 19, no. 2, p. 280, Jan. 2019.
- [38] D. Nemeč, A. Janota, M. Hruboš, and V. Šimák, "Intelligent real-time MEMS sensor fusion and calibration," *IEEE Sensors J.*, vol. 16, no. 19, pp. 7150–7160, Oct. 2016.
- [39] F. O. Silva, R. P. M. Filho, L. A. Vieira, H. K. Kuga, and E. A. de Barros, "Three-axis attitude determination with pseudo-bias estimation from gravity/magnetic vector observations," *J. Guid., Control, Dyn.*, vol. 43, no. 12, pp. 2237–2257, Dec. 2020.
- [40] Y. Yang, F. Li, Y. Gao, and Y. Mao, "Multi-sensor combined measurement while drilling based on the improved adaptive fading square root unscented Kalman filter," *Sensors*, vol. 20, no. 7, p. 1897, Mar. 2020.
- [41] F. Ye, F. Shi, Y. Lai, X. Zhou, and K. Li, "Heading angle estimation using rotating magnetometer for mobile robots under environmental magnetic disturbances," *Intell. Service Robot.*, vol. 13, no. 4, pp. 459–477, Oct. 2020.



YAN XIAOLONG was born in Taiyuan, Shanxi, China, in 1988. He received the B.S. and Ph.D. degrees from the College of Mechatronics Engineering, North University of China, Taiyuan, in 2013 and 2019, respectively. He works at the North University of China and holds a postdoctoral position at Huaihai Industry Group Company Ltd. His current research interests include missile attitude estimation, magnetometer calibration systems, and navigation and guidance theory of missile.



BAI DUNZHUO was born in Hubei, China, in 1989. He received the B.E. degree in weapon system and launch engineering from the College of Mechatronics Engineering, North University of China, Taiyuan, China, in 2012. He works at Yuxi Industry Group Company Ltd., while studying for a Ph.D. degree in weapons and launch engineering. His current research interests include inertial navigation, integrated navigation, and adaptive control.



ZHAO FUCHUN was born in Jilin, China, in 1989. He received the B.E. degree in control engineering from the College of Electronic Information Engineering, Northwestern Polytechnical University, Xian, China, in 2013. He works at Shandong Special Industry Group Company Ltd., while studying for a Ph.D. degree in weapons and launch engineering. His current research interests include inertial navigation, integrated navigation, and adaptive control.



ZHANG WEI was born in Shanxi, China, in 1976. He received the B.E. degree from the College of Mechatronics Engineering, Beijing Institute of Technology, China, in 1989. He is currently a Researcher at Huaihai Industry Group Company Ltd., China. His current research interests include munition damage technology and munition guidance technology.